Biochemistry

pubs.acs.org/biochemistry Article

Catalytic Mechanism of *Mycobacterium tuberculosis* Methionine Sulfoxide Reductase A

Santiago Sastre, Bruno Manta, Jonathan A. Semelak, Dario Estrin, Madia Trujillo, Rafael Radi, and Ari Zeida*

Cite This: https://doi.org/10.1021/acs.biochem.3c00504 Read Online

ACCESS | Metrics & More | Article Recommendations | Supporting Information

ABSTRACT: The oxidation of Met to methionine sulfoxide (MetSO) by oxidants such as hydrogen peroxide, hypochlorite, or peroxynitrite has profound effects on protein function. This modification can be reversed by methionine sulfoxide reductases (msr). In the context of pathogen infection, the reduction of oxidized proteins gains significance due to microbial oxidative damage generated by the immune system. For example, *Mycobacterium tuberculosis* (*Mt*) utilizes msrs (*Mt*msrA and *Mt*msrB) as part of the repair response to the host-induced oxidative stress. The absence of these enzymes makes *Mycobacteria* prone to increased susceptibility to cell death, pointing them out as potential therapeutic targets. This study provides a detailed characterization of the catalytic mechanism of *Mt*msrA using a comprehensive approach, including experimental techniques and theoretical methodologies. Confirming a ping-pong type enzymatic mechanism, we elucidate the catalytic parameters for sulfoxide and thioredoxin substrates (k_{cat}/K_M = 2656 ± 525 s^{-1} M^{-1} and 1.7 ± 0.8 × 10^6 s^{-1} M^{-1}, respectively). Notably, the entropic nature of the activation process thermodynamics, representing ∼85% of the activation free energy at room temperature, is underscored. Furthermore, the current study questions the plausibility of a sulfurane intermediate, which may be a transition-state-like structure, suggesting the involvement of a conserved histidine residue as an acid−base catalyst in the MetSO reduction mechanism. This mechanistic insight not only advances our understanding of *Mt* antioxidant enzymes but also holds implications for future drug discovery and biotechnological applications.

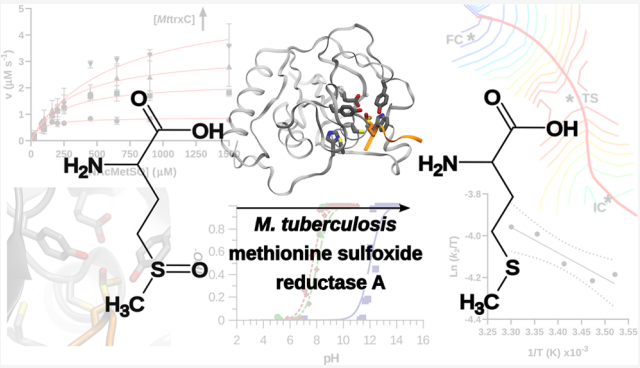

Methionine (Met) oxidation is an important phenomenon not only in redox biology and biochemistry but also in biotechnology, synthetic organic chemistry, physiology, and medicine. It is commonly observed in proteomic cellular approaches, but it is often considered as an artifact of detection techniques. Since the 70s, studies have been reported that methionine residues in proteins can be oxidized to methionine sulfoxide (MetSO) by molecules that are formed *in vivo*, such as hydrogen peroxide (H_2O_2), hypochlorite (HOCl), peroxynitrite (ONOOH), or chloramines (NR_2Cl) suggesting that methionine sulfoxidation is a biologically relevant phenomenon.[1−7] Consistent with their biological relevance, most organisms have MetSO-reducing enzymes called methionine sulfoxide reductases (msr).[8,9] Furthermore, some well-described examples of Met oxidation and reduction regulating important protein activities and cellular functions have been proposed recently.[10−15] Even more, a few examples of enzymes exhibiting methionine oxidase activity have been reported.[16,17] These findings have repositioned this oxidative modification as a new axis of reversible redox regulation, similar to better studied ones such as oxidation and reduction of cysteines.[16]

The noncatalyzed oxidation of Met to MetSO leads to the formation of Met-(*R*/*S*)-SO stereoisomers in equimolar amounts. Six classes of msr are currently known, three bacterial molybdenum-dependent msr,[18] msrP (EC 1.8.5.B1), dmsA (EC 1.8.5.3), and bisC (EC 1.97.1.9), and three thiol-dependent msr, msrA (EC 1.8.4.11), msrB (EC 1.8.4.12), and msrC (EC 1.8.4.14). Peptide methionine sulfoxide reductase A (msrA or PMSR) is a well-conserved enzyme whose function is to reduce the peptide Met-*S*-SO stereoisomer by means of at least one reactive thiol in its active site.[19] Depending on the number and localization of the reactive cysteines, msrA enzymes can be classified as subtype I: one reactive cysteine at position 13; subtype II: two reactive cysteines at positions 51 and 54; subtype III: positions 51 and

Received: September 19, 2023
Revised: December 27, 2023
Accepted: December 27, 2023

Scheme 1. Proposed Elemental Chemical Steps during *S*-Sulfoxide Reduction Catalyzed by msrA

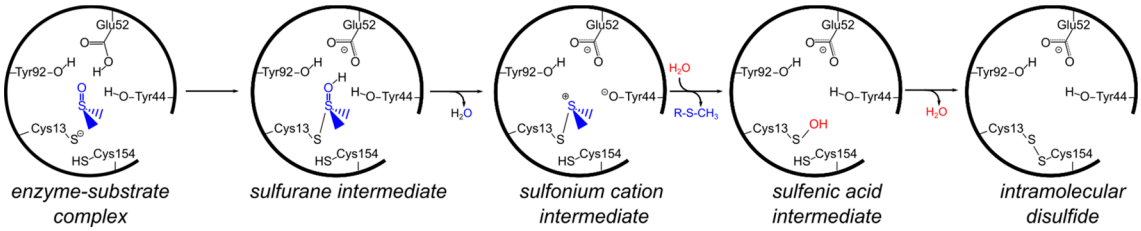

198; and subtype IV: three reactive cysteines at positions 51, 198, and 206 (numbering referred to *E. coli* msrA).

The reduction of oxidized proteins is particularly important in the context of pathogen infection. For example, when macrophages phagocytize mycobacteria, such as *Mycobacterium tuberculosis* (*Mt*), they trigger host activation leading to pathogen exposure to several oxidants, among other immune responses.[20] *Mt* has evolved various survival mechanisms that allow it to efficiently remove these oxidizing species as well as repair systems of oxidized biomolecules.[21,22] In this context, *Mt* expresses two types of peptide methionine sulfoxide reductases, namely *Mt*msrA and *Mt*msrB.[5] Their absence leads to higher reactive oxygen and nitrogen species susceptibility, which makes them potential therapeutic targets.[5,23] These enzymes are proposed to present a bisubstratic ping-pong-like catalytic mechanism. However, the MetSO reduction mechanism of msrAs, and *Mt*msrA in particular, has been a matter of debate in the literature. *Mt*msrA is a member of subtype III msrAs within the above-mentioned classification. Previous theoretical work suggests that the catalytic cycle starts with the nucleophilic attack of the cysteine (Cys) residue on the MetSO, while a conserved glutamic acid (Glu) transfers a proton to the sulfoxide oxygen, forming a sulfurane intermediate, a hypervalent sulfur species.[24−26] The second step consists of a proton transfer by one of the conserved tyrosines (Tyr) at the active site, forming the sulfonium cation.[26,27] This second intermediate would be resolved by a water molecule,[28] releasing the reduced methionine and yielding the experimental reported sulfenic acid.[29] Then, the resolving cysteine attacks the sulfenic acid to form a disulfide.[26,27,29] A detailed overview of these chemical steps and the proposed relevant residues at the active site is presented in Scheme 1. The intramolecular msrA disulfide is finally reduced by the thioredoxin/thioredoxin reductase (trx/TR) system.[30]

Motivated by this compelling redox chemistry, in this work we present a detailed characterization of the catalytic mechanism of *Mt*msrA. To achieve this goal, we employed steady-state and pre-steady-state rapid kinetics determinations, temperature dependence studies, classical molecular dynamics simulations (MD), and hybrid quantum mechanics/molecular mechanics (QM/MM) free energy profile determinations. This allowed us to analyze the entire process with an atomic-detailed and thermodynamic perspective. Our results challenge the previously proposed sulfurane intermediate as a plausible reaction intermediate as well as highlight the role of a conserved histidine (His) residue as an acid−base catalyst in the MetSO reduction mechanism. Overall, this work provides a thorough mechanistic description of an important antioxidant enzyme in *Mt* with potential applications in drug discovery and biotechnology.

METHODS

Experimental Methods. *Materials.* Dithiothreitol (DTT), reduced nicotinamide adenine dinucleotide phosphate (NADPH), isopropyl-*β*-D-thiogalactopyranoside (IPTG), ampicillin, 2-iodoacetamide, diethylenetriaminepentaacetic acid (DTPA), and imidazole were purchased from Sigma-Aldrich (Darmstadt, Germany). N-acetyl-L-methionine (NAcMet), MetSO, and N-acetyl-L-methionine sulfoxide (NAcMetSO) were obtained from Bachem (Torrance, USA). All other reagents were obtained from standard commercial sources and used as received. Unless otherwise indicated, experiments were performed in 20 mM Tris buffer plus 0.1 mM DTPA, pH 7.4, and 25 °C.

Enzyme Expression and Purification. The gene encoding *Mt*msrA (TB Database: Rv0137c, UniProt: P9WJM5, 21 kDa) fused at the C-terminal to maltose-binding protein (MBP, 43 kDa) and an N-terminal poly-His tag was cloned in a pDEST17 vector. The fusion protein was expressed in *Escherichia coli* BL21(DE3) grown in LB medium in the presence of ampicillin (100 mg L^{-1}) at 37 °C. The expression of the enzyme was induced by the addition of 1 mM IPTG overnight at 20 °C. The centrifuged bacteria were resuspended in 40 mL of 20 mM Tris buffer, 0.5 M NaCl pH 7.6 (solution A) for each liter of culture. The sonicated bacteria were filtered (0.8 μm) and passed through a nickel HisTrap column equilibrated in solution A and 5 mM imidazole, and the fusion protein was eluted with a linear gradient of imidazole. The poly-Hys and MBP were then cleaved by incubation with the recombinant TEV protease in a 1/10 molar ratio overnight at 4 °C. After proteolysis, proteins were separated by means of a second affinity chromatography using a nickel HiTrap column (GE Healthcare). The fusion protein and *Mt*msrA concentration was measured by absorbance at 280 nm by using a molar extinction coefficient of 100 395 M^{-1} cm^{-1} and 34 045 M^{-1} cm^{-1} respectively, calculated from their sequences in their reduced form (https://web.expasy.org/protparam/). Protein thiol contents were measured by the Ellman's assay ($\varepsilon_{412\ nm}$ = 14 150 $M^{-1}cm^{-1}$).[31] An SDS-PAGE gel of the purification process is depicted in Figure S1a.

Thioredoxin reductase 2 from *Pseudomona aeruginosa* (*Pa*TR, UniProt: Q9I592) gene fused to an N-terminal poly-His tag was cloned in a pET28A vector. The expression and purification conditions were analogous to those of *Mt*msrA, without the need of proteolysis.

*Mt*trxC (UniProt: P9WG67) and *Ec*Trx1 (UniProt: P0AA25) were expressed recombinantly and purified as described before.[32,33]

Steady-State Kinetics Assay. *Mt*msrA activity was assessed by steady-state kinetics by following the decrease in the absorbance of NADPH at 340 nm ($\varepsilon_{340\ nm}$ = 6220 M^{-1} cm^{-1}) due to its oxidation in a coupled assay. The protein and substrate concentration were 200 μM NADPH, 2 μM *Pa*TR, a

https://doi.org/10.1021/acs.biochem.3c00504
Biochemistry XXXX, XXX, XXX−XXX

variable range of 5−80 μM *Mt*trxC (or *Ec*Trx1), and a variable range of 0−1500 μM NAcMetSO or MetSO. All experiments were performed at 25 °C. Primary records of initial velocity were plotted as a function of substrate in different concentrations of *Mt*trxC during the experiment. Experimental data were fitted to the Michaelis−Menten rate equation obtaining V_{max}^{app} and $K_{0.5}^{app}$. Secondary graphics were then built to observe the dependence of each parameter on the other substrate, calculating K_M and k_{cat} of the enzyme for each substrate. Activity measurement controls are presented in Figure S1b.

Pre-Steady-State Kinetics. The oxidation rate constants of *Mt*msrA by MetSO or NAcMetSO were determined by measuring the decrease in the intrinsic protein fluorescence intensity (λ_{ex} = 295 nm) upon oxidation. Prereduced *Mt*msrA, typically 1 μM, was rapidly mixed with excess sulfoxide using a stopped flow spectrophotometer (Applied Photophysics SX20). The observed rate constants of fluorescence decay (k_{obs}) were determined by fitting a monoexponential function to the experimental data. The second order rate constants of the reactions were obtained from the slope of the linear regression of k_{obs} versus sulfoxide concentration in a variable range of 0−5 mM. To obtain the thermodynamic activation parameters of oxidation of *Mt*msrA by NAcMetSO, the experiment was carried out at four different temperatures (14.9, 20.0, 25.0, and 30.0 °C), and Arrhenius or Eyring analyses were performed.

Circular Dichroism and Melting Temperatures. Changes in the secondary and tertiary structure content of *Mt*msrA were followed by the circular dichroism (CD) signal in the far-UV (195 to 260 nm) using a 1.0 mm path-length cell and in the near-UV (240 to 350 nm) using a 1 mm path-length cell. Measurements were made in an Applied Photophysics Chirascan V100. *Mt*msrA (10 μM final concentration) was prepared in 20 mM Tris-HCl, 1 mM DTPA pH 7.4. Both reduced and oxidized states were obtained by incubating the protein samples for 30 min at room temperature in the presence of 2 mM DTT or 1 mM NAcMetSO, respectively. After that, excess DTT or NAcMetSO was removed with a desalting column. At least 10 spectra were acquired with a speed scan of 50 nm min^{-1}. The blanks/buffer spectra were acquired and subtracted from the average protein spectrum. Melting temperatures of both reduced and oxidized enzymes were estimated by collecting far-UV DC spectra between 20.0 and 65.0 °C.

Computational Methods. *Classical and Hybrid QM/MM Molecular Dynamic Simulations. System Preparation.* Every initial system was prepared from the crystallographic structure of *Mt*msrA in complex with a peptidic Met bound in the active site coming from an *Mt*msrA crystallographic image (PDBid 1NWA).[34] When modeling substrate or product bound to *Mt*msrA, the first six amino acids were kept (His−Met−Thr−Ser−Asn−Gln); therefore, Met*2 would be the reducible MetSO substrate. After removing the crystallographic water, hydrogen atoms were added by using the *tleap* module of the AMBER18 suite,[35] leaving the titratable residues as expected at physiological pH of 7.4. All systems were embedded in a truncated octahedral TIP3P water box, extended 12 Å from any protein atom.

Molecular Dynamics Simulation Protocol. All systems were subjected to the same MD protocol and sampling. Energy minimization and conventional molecular dynamics simulations (MD) were conducted applying the *ff*14SB force field[36] to all standard residues, and parameters for methionine sulfoxide, methionine sulfonium, and sulfenic acid were generated by using the RESP protocol[37,38] and the *gaff* force field.[39] A two-step minimization protocol was used, relaxing first all water molecules for 2000 steps (2000 steepest descent, SD) keeping the protein by a 10 kcal mol^{-1} $Å^{-2}$ restraint. 3000 additional minimization steps (1000 SD; 2000 conjugated gradient, CG) were performed then on the whole system. The system was heated to 300 K in 0.5 ns long MD followed by NPT simulation to adjust the system to the corresponding density at 300 K. Finally, production MDs on the NPT ensemble were performed. Temperature and pressure control were exerted by using the Berendsen thermostat and the Monte Carlo barostat (10 ps pressure-coupling constant). A 10 Å cutoff was applied to nonbonded interactions, and long-range electrostatics were treated under periodic boundary conditions (PBC) with the particle-mesh Ewald (PME)[40] procedure with a grid spacing of 1 Å. The SHAKE protocol[41] was applied to hydrogen atom bonding, and an integration time step of 2 fs was used. A detailed description of each simulated system is presented in Table S1.

pH Titration Molecular Dynamics. The pK_a of Glu52, Tyr44, Tyr92, and His155 was estimated through constant pH titration molecular dynamics (pHtMD). This protocol consisted of an adaptation of the original method developed by Socher & Sticht.[42] In brief, *Mt*msrA was simulated at a fixed pH for 10 ns using MD. A second simulation was then initiated using the coordinates and velocities from the previous simulation but with the pH increased by 0.2 units. During the simulation, the protonation state of these residues was monitored by Monte Carlo sampling of the Boltzmann distribution of protonation states, as implemented in the AMBER package. For example, the fraction of deprotonated Glu52 ($f_{deprotonated}$) was calculated from the total number of frames at each pH in which Glu52 was deprotonated, and the pK_a was finally determined from the following equation:

$$f_{deprotonated}(\mathrm{pH}) = \frac{1}{1 + 10^{\mathrm{pK_a} - \mathrm{pH}}} \quad (1)$$

QM/MM Molecular Dynamics and Umbrella Sampling Protocol. The LIO software was used to perform QM/MM simulations.[43,44] Three water molecules, the side-chains of residues Cys13, Glu52, Tyr44, Tyr92, His155, and Met*2, were included in the QM subsystem depending on the distinguished coordinate. The QM region was modeled using both the PBE[45] exchange and correlation functional combination with a dzvp basis set and the MM region with the ff14SB force field.[36] Free energy profiles were constructed by the umbrella sampling approach,[46] using similar protocols as before.[47,48] Briefly, the initial structures were generated from previous MD simulations in an 18 Å truncated octahedral box with periodic boundary conditions. Then, a steered QM/MM molecular dynamics simulation was carried out in order to span the entire selected coordinate range. To relax the initial structure, a QM/MM equilibration protocol was employed, involving three steps: (1) changing charge parameters in the classical residues of the QM subsystem, (2) alternating classical MD simulations of the system fixing the QM region with short QM optimizations on the QM region with the fixed MM region, and (3) modifying the topology using optimized parameters. This protocol was iterated 10 times for each window. After the final thermalization, these structures were used as the starting coordinates for each umbrella sampling

https://doi.org/10.1021/acs.biochem.3c00504
Biochemistry XXXX, XXX, XXX−XXX

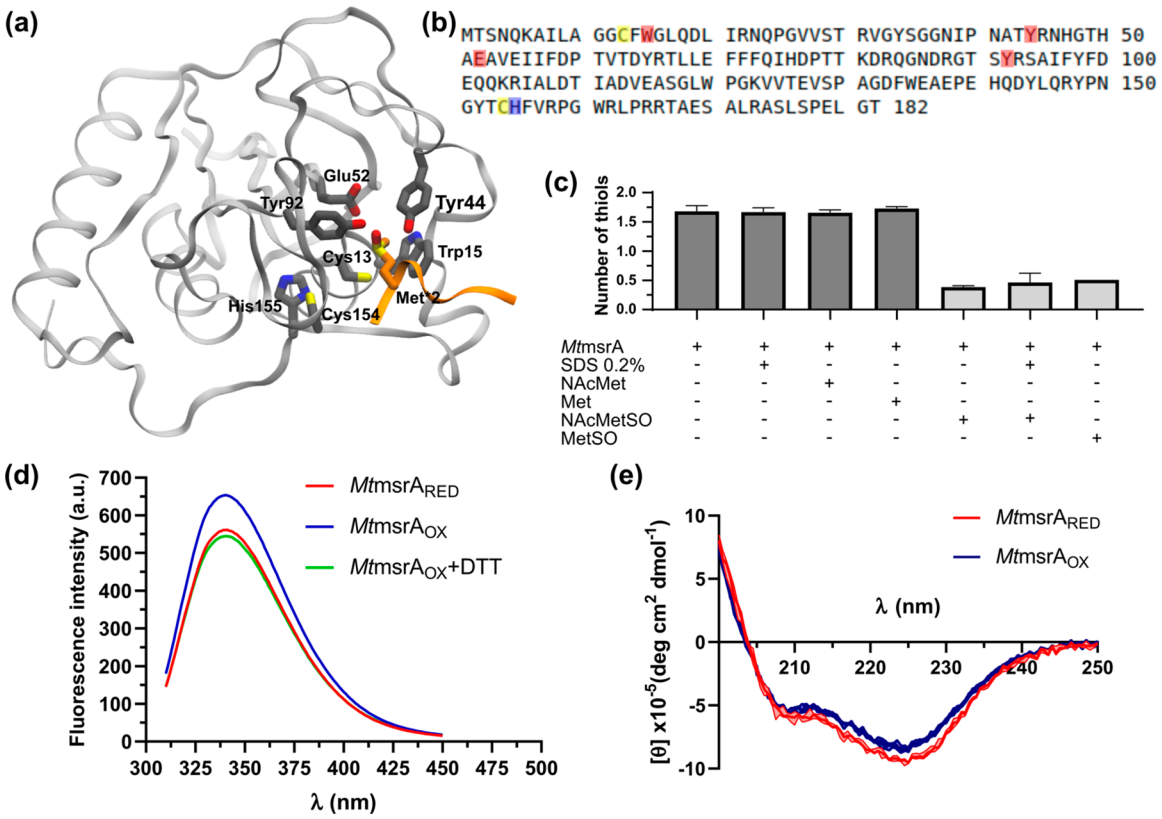

Figure 1. *Mt*msrA structure, sequence, and changes associated with its redox state. (a) Structure of our *Mt*msrA−substrate model and (b) *Mt*msrA sequence, highlighting active site important residues. (c) Enzyme free thiol quantification by Ellman's assay in different conditions. Light gray bars correspond to samples preincubated with substrate. (d) Fluorescence emission spectra (λ_{ex} = 295 nm) of reduced *Mt*msrA (red), oxidized *Mt*msrA (blue), or after the addition of 2 mM DTT to oxidized *Mt*msrA (green). (e) Circular dichroism far-UV spectra (deg cm^2 dmol^{-1} × 10^{-5}) of reduced *Mt*msrA (red), oxidized *Mt*msrA (blue).

window. Each simulation window was followed by a 5 ps uncoupled thermostat QM/MM simulation and a 10 ps Langevin thermostat simulation. Only the Langevin MD trajectories were used for analysis.

Visualization and molecular drawings were made using VMD 1.9.1,[49] numerical data analysis, fittings, and plots were performed using QtiPlot.

■ RESULTS AND DISCUSSION

Structural and Dynamic Characterization of *Mt*msrA.

The dynamic and structural behavior of *Mt*msrA was analyzed in both the oxidized and reduced states. Its structure is depicted in Figure 1a. The enzyme possesses two Cys residues in its sequence, the nucleophilic Cys13 and the resolving Cys154 (Figure 1b). The number of reduced thiols in different redox states was determined using Ellman's assay[31] (Figure 1c). After reduction with DTT, approximately 1.8 free thiols per mole of protein were detected, a slightly lower value than expected. When an excess of substrate was added to the reduced protein, only 0.4 thiols per mole of protein were detected, suggesting that most thiols are oxidized to disulfide.

The intrinsic fluorescence emission and circular dichroism spectra of the protein are sensitive to its redox state, as has been previously reported for *Nm*msrA.[27] In Figure 1d, an increase in intrinsic fluorescence is observed upon protein oxidation, and this change can be reversed by adding excess DTT to the oxidized protein. Additionally, oxidation leads to a subtle decrease in the protein secondary structure content (Figure 1e).

Since the chemical reaction would start by the protonation of the sulfoxide moiety and the nucleophilic attack of Cys13 in its thiolate state, we evaluated how protonation states and the presence/absence of substrates/products affect the reduced *Mt*msrA structure and dynamics and specifically how the active site microenvironment responded to these changes. Therefore, the dynamic properties of several protein and peptide−protein complexes, considering different protonation states of Cys13 and Glu52, were studied using MD. The results are summarized in Figure 2.

The binding of peptide substrates with or without an oxidized methionine increases protein flexibility in the regions near the active site, as shown by the increase in the C_α RMSF in these areas in Figure 2a,b. Previous biochemical studies have demonstrated the importance of several conserved residues at the msrA active site.[27,50−53] The interaction between the sulfoxide and these residues at the active site was analyzed by calculating distance distributions of Met*2Oε and the functional groups of Glu52, Tyr44, and Tyr92. These distance distributions showed a shift toward a reactive conformation when Glu52 was modeled as glutamic acid (Figure 2d). The pK_as of Glu52, Tyr44, and Tyr92 were measured using pHtMD and were found to be 11.8, 7.7, and 12.6, respectively (Figures 2c and S2). When the pK_a of Glu52 was measured in the presence of substrate, it shifted 4 pH units to alkaline pH (from 7.7 to 12), but this increase was not observed in the presence of the product, resulting in a similar pK_a value as the free enzyme, strongly suggesting that the sulfoxide oxygen atom generates changes in the electrostatic properties of the

https://doi.org/10.1021/acs.biochem.3c00504
Biochemistry XXXX, XXX, XXX−XXX

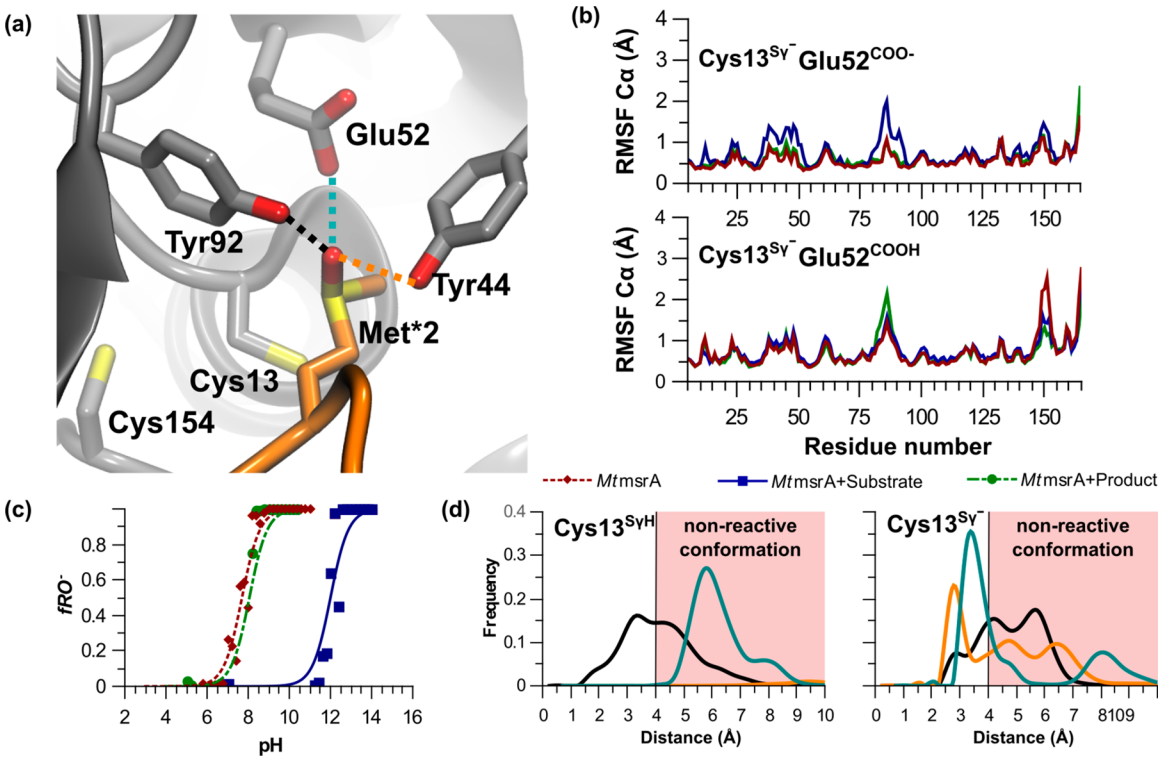

Figure 2. Dynamical behavior of reduced *Mt*msrA and its Michaelis complexes. (a) Active site representation of *Mt*msrA in the presence of substrate. (b) C_α root-mean-square fluctuation (RMSF, Å) of *Mt*msrA with Glu52 deprotonated or protonated. (c) Glu52 titration simulation curves, as its deprotonated fraction (fRO^-) versus pH. In (b) and (c), results for the *Mt*msrA, *Mt*msrA + substrate, and *Mt*msrA + product are depicted using red, blue, and green lines, respectively. (d) Distribution of the active site interaction distances (Å) between Met*2$^{O\varepsilon}$−Glu52$^{O\varepsilon}{}_{COOH}$ (blue-green), Met*2$^{O\varepsilon}$−Tyr44^{OH} (orange), and Met*2$^{O\varepsilon}$−Tyr92^{OH} (green) along the MD with C13$^{S\gamma H}$ (left) or C13$^{S\gamma-}$ (right).

active site resulting in an anomalous Glu52 pK_a.[53] In summary, binding of the substrate into the active site promotes protonation of Glu52, favoring the interaction of the sulfoxide in a reactive pose (see below).

Steady-State Kinetic Characterization of *Mt*msrA. The steady-state enzyme kinetics was studied by monitoring NADPH oxidation in a coupled assay, as described in the methodology section (Figure 3a). The catalytic parameters obtained for NAcMetSO were K_M = (1.36 ± 0.16) mM and k_{cat} = (3.7 ± 0.3) s^{-1} (Figure 3b,c). These values are consistent with previous reports.[27] The K_M for *Mt*TrxC was (20 ± 7) μM, slightly higher than that reported K_M for *Ec*Trx1 in *Ec*msrA.[54] The k_{cat}/K_M was (2656 ± 525) s^{-1} M^{-1} and (1.7 ± 0.8) × 10^6 s^{-1} M^{-1} for NAcMetSO and *Mt*TrxC, respectively, both of which are in line with previous reports on bacterial msrAs as reported in Table S2.

The hyperbolic dependence of the kinetic parameters against the [NAcMetSO] or [*Mt*trxC] observed in Figure 3d,e confirmed the ping-pong bisubstrate mechanism proposed for this family of enzymes.[54] The linearization of the Michaelis curves is also consistent with a ping-pong mechanism (Figure S1d). When we tested *Ec*trx1 as an *Mt*msrA reductant in order to compare its activity with *Mt*trxC, we observed a 40% decrease in total activity (Figure S1b).

Molecular Basis of Sulfoxide Reduction by *Mt*msrA. The change in the intrinsic fluorescence of *Mt*msrA associated with its redox state (Figure 1d) allowed us to study the pre-steady-state kinetic properties of sulfoxide reduction by *Mt*msrA by following the increase in total fluorescence in a stopped flow apparatus (Figure 4a,b). Furthermore, through the evaluation of the k_2 temperature dependence, we were able to estimate the thermodynamic activation parameters (Figure 4c and Table 1).

The NAcMetSO reduction rate constant at pH 7.4 and 25 °C is 4.6 s^{-1} mM^{-1}, almost 2 times larger than the one determined for MetSO (Figure S3). The reported k_2 value for *Neisseria meningitidis* (*Nm*) msrA is 1.5 s^{-1} mM^{-1}, which is approximately half that of the k_2 value for *Mt*msrA.[27,50]

The activation energy and activation enthalpy determined by Arrhenius and Eyring analyses highlight the predominant entropic contribution in the activation process energetics. The enthalpic contribution is close to the accessible energy at relevant temperatures but ∼6 times lower than the entropic contribution at 25 °C.

To shed light into the molecular basis of the sulfoxide reduction process and rationalize the thermodynamic activation parameters obtained, we conducted a series of reaction potential and free energy estimations, using both purely QM electronic structure calculations and QM/MM molecular dynamics simulations. The magnitude of the entropic contribution observed in the activation parameters underlines the importance of exhaustively treating the dynamical aspects of the process. We found that reducing the sulfoxide, releasing the reduced Met, and forming the disulfide bond between the nucleophilic and resolution Cys residues involve three elemental reactions at the enzyme's active site.

Figure 5a shows the free energy profile of the first step, involving the first two elemental steps depicted in Scheme 1, obtained by QM/MM umbrella sampling simulations. The profile exhibits four chemically significant regions (Initial Complex IC, Transition State TS, "Bump" BU, and Final

https://doi.org/10.1021/acs.biochem.3c00504
Biochemistry XXXX, XXX, XXX−XXX

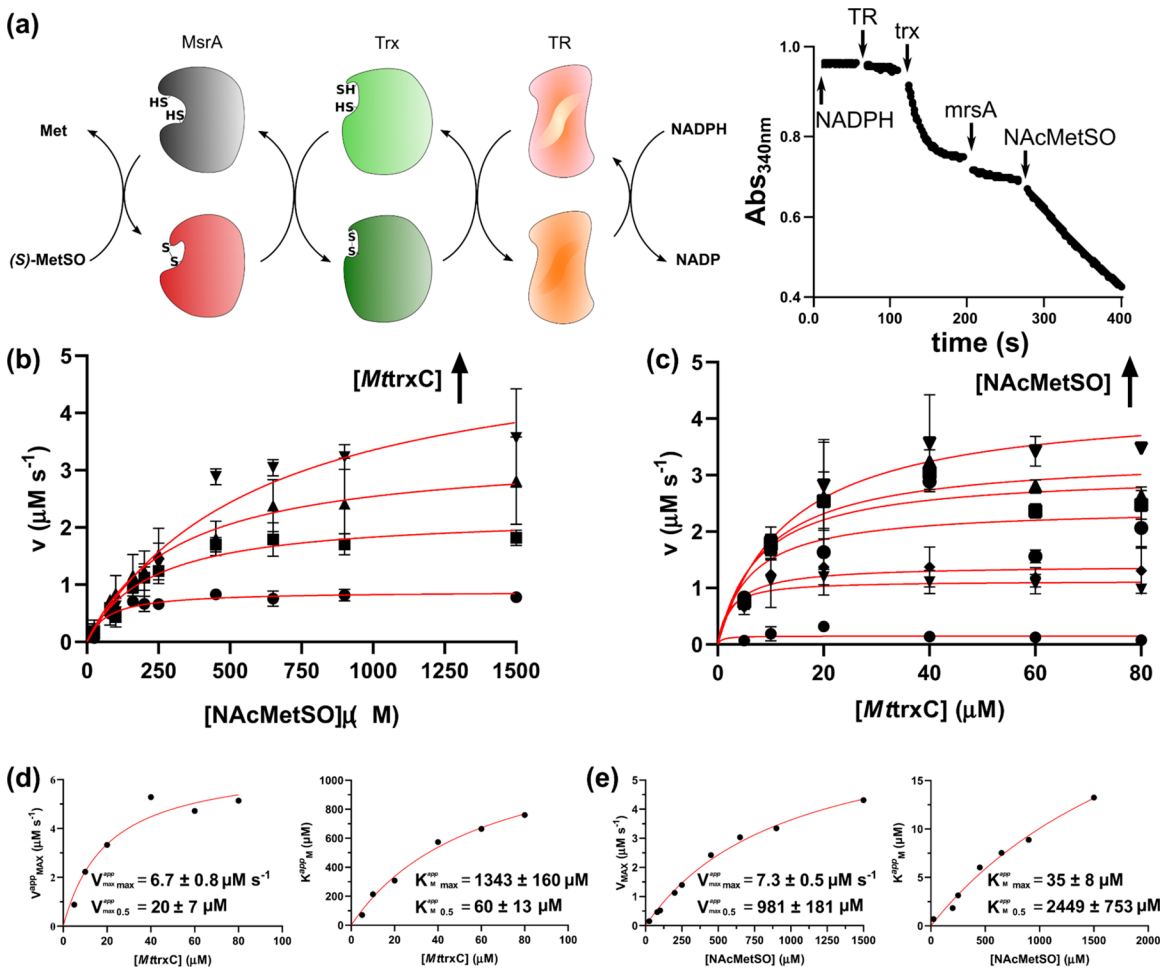

Figure 3. Enzymatic activity of recombinant *Mt*msrA. (a) Scheme of the electron flux along the coupled assay and a representative temporal course of absorbance at 340 nm. (b) Michaelis−Menten analysis of NAcMetSO (0−1500 μM) reduction by *Mt*msrA at different *Mt*trxC (5−80 μM) concentrations or (c) *Mt*trxC (5−80 μM) at different NAcMetSO (0−1500 μM) concentrations. (d,e) Apparent kinetic parameters' dependence on substrate concentrations from (b) or (c), respectively. All of the experiments were performed at least three times, at pH 7.4, 25 °C, *Pa*TR 2 μM, and NADPH 200 μM.

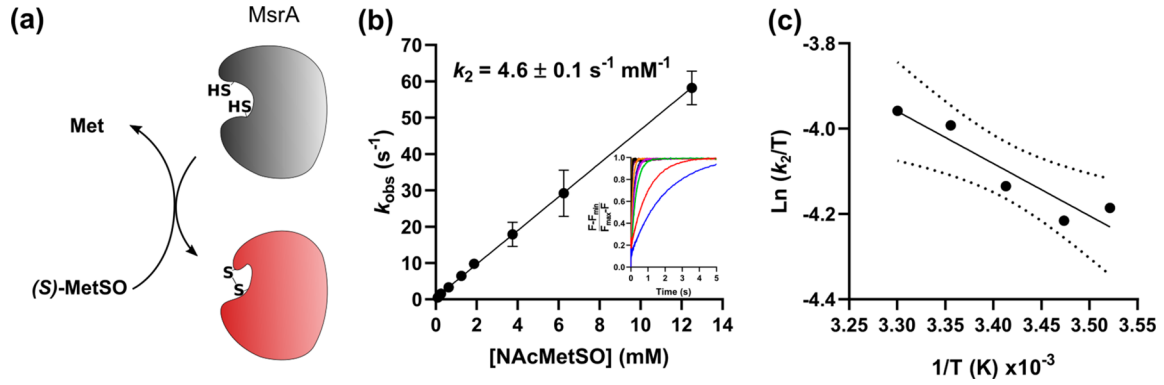

Figure 4. Pre-steady-state kinetic analysis of NAcMetSO reduction by*Mt*msrA. (a) Scheme of the reaction in the prestationary kinetic experiments. (b) Time courses of the oxidation kinetics of *Mt*msrA by NAcMetSO at 25 °C (inset). k_{obs} were determined from fitting monoexponential functions to the temporal courses, and k_2 was estimated from the slope of k_{obs} as a function of substrate concentration. (c) Eyring analysis of k_2, independently determined three times for each temperature.

Complex FC), the representative structures of which are depicted in Figure 5b. These structures are similar to the stationary points obtained by QM calculations in reduced cluster models comparing different DFT functionals, as shown in Figure S4a and Table S3. The free energy profile maximum corresponds to an early TS, in which the first proton is being transferred to the sulfoxide O atom and the thiolate in Cys13 is starting the attack on the Met*2$^{S\delta}$ atom (Figure 5c). Also, the energy profile shows a distinctive bump at ∼−0.5 Å of the reaction coordinate, whose structure resembles the TS from

https://doi.org/10.1021/acs.biochem.3c00504
Biochemistry XXXX, XXX, XXX−XXX

Table 1. Kinetic and Thermodynamic Parameters from NAcMetSO Reduction by *Mt*msrA

$k_2^{25°C}$ (s^{-1} M^{-1})	E_{act} (kcal mol^{-1})	$\Delta^{\ddagger}H$ (kcal mol^{-1})	$\Delta^{\ddagger}S$ (cal mol^{-1} K^{-1})	$\Delta^{\ddagger}G_{25\ °C}$ (kcal mol^{-1})
4.6×10^3	3.7	2.4	−46.0	16.1

the nucleophilic attack and coincides with the proton transfer from Tyr44/Tyr92 to the OH^- leaving group from the cluster model, as shown in Figure S4b and Table S3. Both the TS and BU regions resemble the previously reported sulfurane catalytic intermediate, but our simulations suggest that these species are not minima in the free energy surface. Thiriot and colleagues studied the complete catalytic mechanism by employing an active site cluster model.[25] Their work did not reveal any free energy differences between the transition state and the sulfurane intermediate, which was found to be even less stable than the transition state of the second step in the presence of solvent, as reported in his work.[25] Dokainish and co-workers estimated a $\Delta^{\ddagger}G$ of 2.3 kcal mol^{-1} for the first step, which is a small energy difference that can be attributed to the roughness of the potential energy surface.[26] To further evaluate the stability of the proposed sulfurante intermediate, we conducted unrestricted QM/MM MD simulations starting from these points (TS and BU), resulting in the system shifting to IC and FC, respectively (Figure 5b), confirming that neither of those species represents a minimum in our free energy surface.

MD simulation of the sulfonium cation intermediate was performed to characterize the dynamics of this species and the changes that can be exerted at the active site. The evolution of sulfonium to sulfenic acid has been demonstrated to proceed via hydrolysis,[53] so solvation properties of active site residues are of particular importance in this intermediate state. Cys13 and His155 solvation analyses are displayed in Figure 6a,b. Cys13 was found to interact with His155 through two water molecules, a configuration observed in ∼40% of the simulation. This arrangement is very favorable for coupling acid−base catalysis with the nucleophilic attack of a water molecule on the sulfonium. We tested this mechanistic hypothesis by determining the free energy profile of this second step, implementing a 2D umbrella sampling approach to adequately sample the proton relays between His155, water molecules, and Cys13 (Figure 6c). In order to characterize the acid−base properties of His155, we performed constant pH MDs to estimate the titration curves of this residue in several intermediary states of the reaction mechanism (Figure S5). Interestingly, we found that the His155 pK_a is quite sensitive to the microenvironment of the active site and presents a much lower pK_a value when the sulfonium cation is present than in any other active site state.

The free energy surface in Figure 6c provides information about the minimum free energy path connecting the sulfonium cation intermediate with the sulfenic acid (second elemental chemical step in Scheme 2), showing a free energy barrier and reaction free energy of approximately 5.5 kcal mol^{-1} and −6.0 kcal mol^{-1}, respectively. The stationary points along the path are shown in Figure 6d. At the TS, the nucleophilic attack is tightly coupled with an acid−base catalysis mechanism. Once the protons are transferred, the free energy drops rapidly, suggesting that His155 plays a dual role in providing both specific and general acid−base catalysis,[55] allowing for the resolution of the sulfonium intermediate.

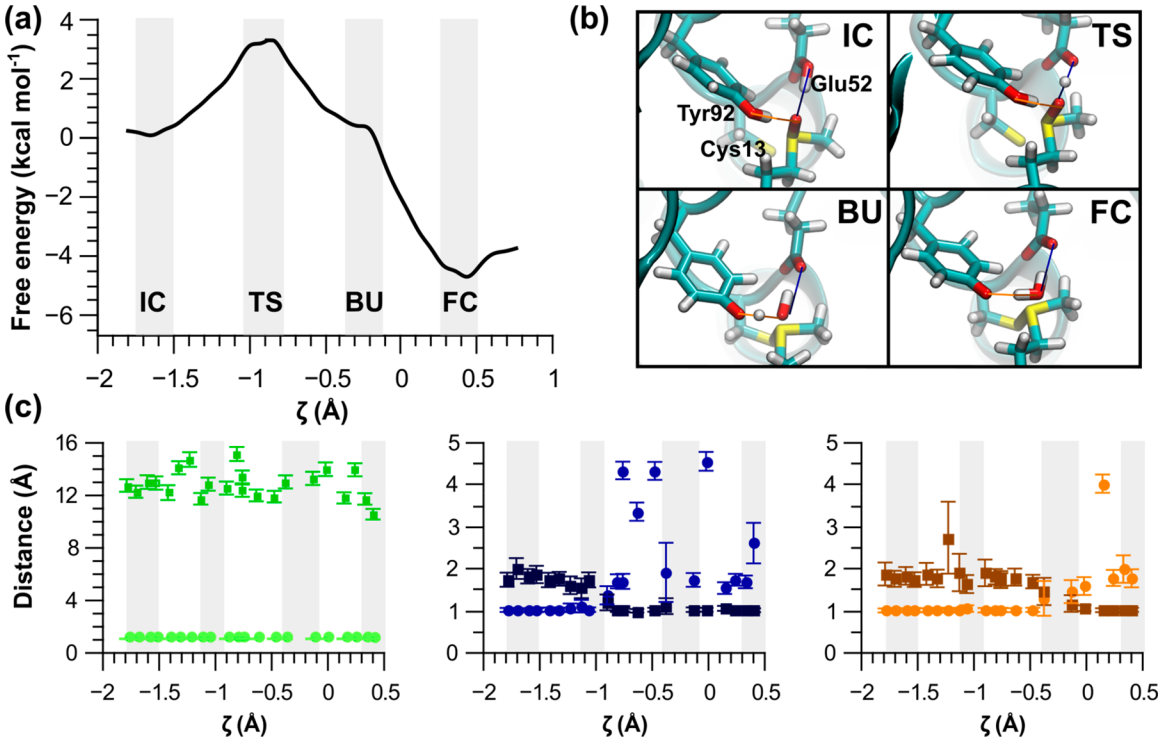

Figure 5. Analysis of the free energy profile and relevant distances in the first step. (a) Free energy profile as a function of ζ(Å) defined as the difference between $Cys13^{S\gamma}$−$Met{*}2^{S\delta}$ and $Met{*}2^{S\delta}$−$Met{*}2^{O\varepsilon}$ distances. (b) Representative structure of the different stationary points detected in the free energy profile. IC, TS, BU, and FC refer to Initial Complex, Transition State, Bump, and Final Complex (see the text). (c) Distance evolution of $Tyr44^{OH}$−$Tyr44^{HO}$ (green circle), $Tyr44^{HH}$−$Met{*}2^{O\varepsilon}$ (green square), $Glu52^{O\varepsilon H}$−$Glu52^{HO\varepsilon}$ (blue circle), $Tyr44^{HH}$−$Met{*}2^{O\varepsilon}$ (black square), $Tyr92^{OH}$−$Tyr92^{HO}$ (orange circle), and $Tyr92^{HH}$−$Met{*}2^{O\varepsilon}$ (brown square).

https://doi.org/10.1021/acs.biochem.3c00504
Biochemistry XXXX, XXX, XXX−XXX

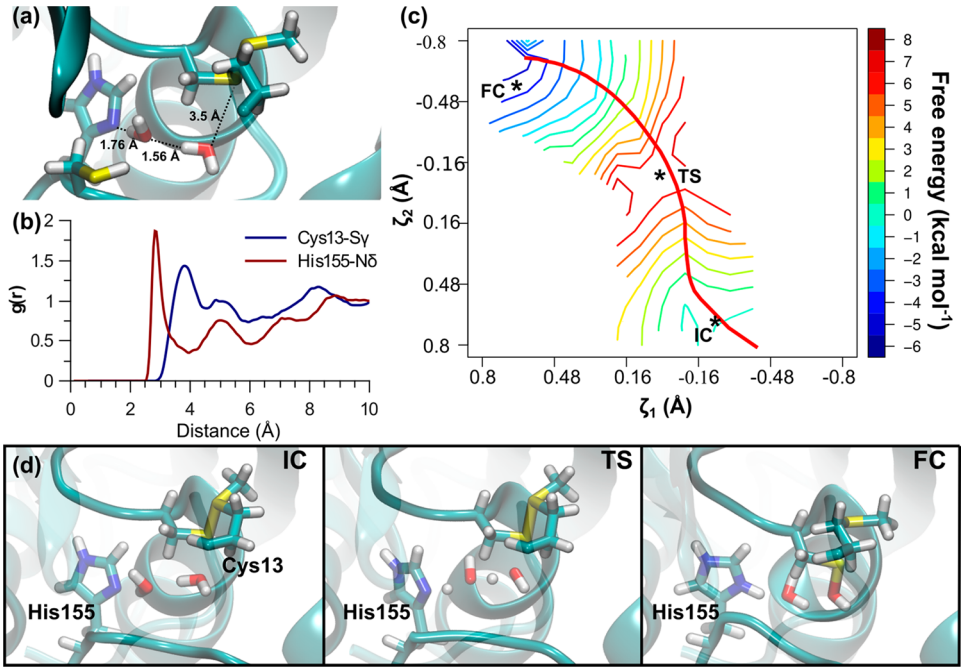

Figure 6. Dynamical behavior of sulfonium cation and its resolution. (a) Representative structure of the active site along the molecular dynamics of the sulfonium cation intermediate state. (b) Radial distribution function of water molecules around $Cys13^{S\gamma}$ and $His155^{N\delta}$ along the simulation. (c) Free energy surface (color scale, kcal mol^{-1}) of the second step. ζ_1 (Å) is defined as the difference between $Cys13^{S\gamma}$−H_2O^O and $Cys13^{S\gamma}$−$Met{*}2^{S\delta}$ distances and ζ_2 (Å) as the difference between $His155^{N\delta}$−H_2O^H and $H2O^H$−H_2O^O distances. (d) Representative structures of selected points (asterisks in panel c) at the free energy surface which represent the initial complex (IC), the transition state (TS), and the final complex (FC).

Scheme 2. Elemental Chemical Steps of *S*-Sulfoxide Reduction Catalyzed by *Mt*msrA

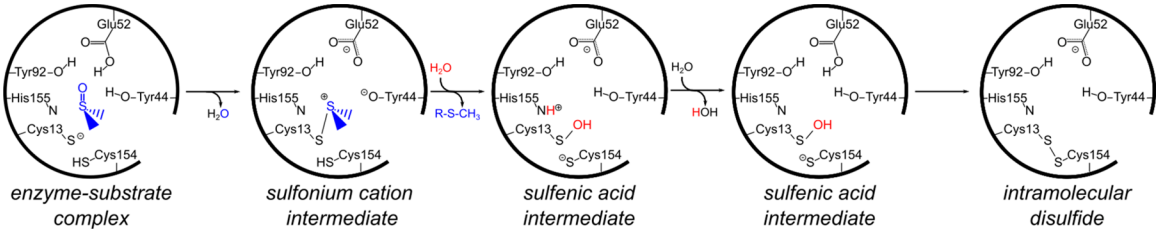

Then, we addressed whether this mechanistic proposal could be extrapolated to other msrA members. Catalytic residues Tyr44, Glu52, and Tyr92 are all present in the msrA sequences. However, the conservation of cysteine residues is less clear, which is why msrA was subdivided based on its biochemical properties outlined in the Introduction rather than on a phylogenetic criterion. To gain a deeper understanding of the conservation of His155, the frequency of its appearance at this position was analyzed (Figure S6a,b). The results showed that the level of conservation of His155 in msrA sequences is 25.8%, with significant variations depending on the type of msrA. In particular, subtype III (to which *Mt*msrA belongs) exhibits a high level of conservation for this His residue (60.7%). Additionally, the distribution of different msrA subtypes along the evolutionary tree was also investigated (Figure S6c). When looking at residue conservation within the msrA type III subtype, Gly is the more represented amino acid in the 40% of sequences where His is not present at position 155. Furthermore, in other msrA subgroups, His is also not well-conserved at that position. Two main possibilities appear to overcome the need of acid−base catalysis: the first one is the possibility of Glu52 also having an acid−base catalysis role not only in the first step of the reaction, as previously discussed; and the second one would be the participation of specific water molecules at the active site that could perform this task. This last hypothesis is partially supported by MD simulations of the sulfonium cation state, where several specific interactions between active site residues and water molecules are observed (Figure 6b and 6b). Deeper evolutionary and mechanistic analysis is needed, but our data point to this His residue as an important catalytic amino acid, at least for this msrA subtype.

Resolution of sulfenic acid to a disulfide bond requires an acid catalyst due to the high basicity of the hydroxyl group as the leaving group, as the reactive species are the protonated sulfenic acid and the corresponding resolving thiolate.[56,57] A close inspection of the active site dynamical properties when sulfenic acid is present at Cys13 suggests two candidates for this task: Glu52 or His155. We previously showed how Glu52 neutral state is favored in *Mt*msrA active site (Figure 2d). On top of that, the orientation of both reactive Cys (13 and 154) and both reactive Cys seem to be more reaction-prone oriented when Glu52 is in this neutral state (Figure S7). Thus, we decided to compute the free energy profile modeling Glu52 as glutamic acid.

https://doi.org/10.1021/acs.biochem.3c00504
Biochemistry XXXX, XXX, XXX−XXX

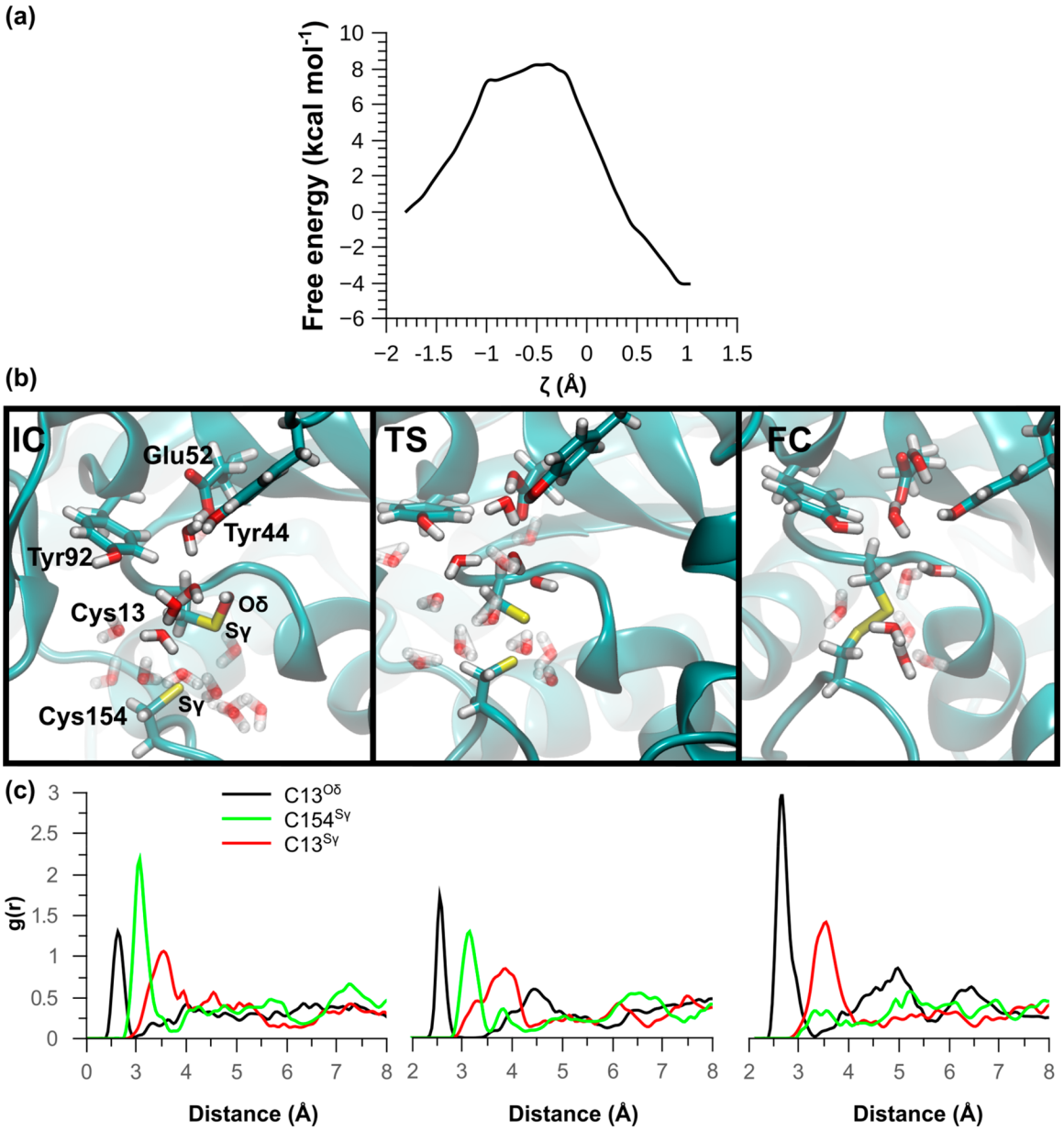

Figure 7. Sulfenic acid resolution. (a) Free energy profile (kcal mol^{-1}) of the disulfide bond formation as a function of the distinguished coordinate ζ (Å), defined as the difference between Cys13$^{S\gamma}$−Cys13$^{O\delta}$ and Cys13$^{S\gamma}$−Cys154$^{S\gamma}$ distances. (b) Representative structures of the IC (initial complex), TS (transition state), and FC (final complex), respectively. (c) Radial distribution function of Cys13$^{S\gamma}$, Cys13$^{O\delta}$, and Cys154$^{S\gamma}$ with water molecules for each selected state.

The free energy profile of this third step (see the last step in Scheme 2) has a free energy barrier and reaction free energy of 8.2 kcal mol^{-1} and −4.1 kcal mol^{-1}, respectively, indicating that it is an exergonic process (Figure 7a). Although in this case it was not possible to properly sample the proton transfer, since it occurs after the maximum of the free energy profile, it is probably not affecting the free energy barrier estimation. The solvation profiles of the atoms involved in the reaction change significantly, as can be seen in Figure 7b,c. Initially, the Cys154$^{S\gamma}$ atom has the largest and most defined solvation structure compared to the Cys13$^{S\gamma}$ and Cys13$^{O\delta}$ atoms. At the transition state, the peak height associated with the number of water molecules in the first solvation sphere of Cys154$^{S\gamma}$ decreases by half, while the peak height associated with the Cys13$^{O\delta}$ atom increases.

In summary, through a combination of kinetic assays and simulations, we have investigated the process of sulfoxide reduction in *Mt*msrA. An updated version of the oxidative part of the catalytic mechanism is presented in Scheme 2. Our results highlight the existence of three elementary reactions once the substrate reaches the enzyme's active site, which are involved in sulfoxide reduction and disulfide bond formation. The experimental activation free energy is higher than the computationally obtained values for the elementary steps. This barrier underestimation may be attributed, at least in part, to well-described DFT flaws (pure functionals in particular) in these regards[58] (Table S3). Considering only the different steps of the oxidative part of the catalytic cycle, the formation of the disulfide bond (last step in Scheme 2) has a larger activation free energy. The rate-limiting step, however, is not only determined by the activation energy or rate constant of

https://doi.org/10.1021/acs.biochem.3c00504
Biochemistry XXXX, XXX, XXX−XXX

the individual reactions, but in the case of bimolecular reactions as the first stages of the mechanism, also by reactant concentrations. Considering that the free energy barriers determined herein are similar and that every reasonable scenario would display oxidizing substrate concentrations in the mM range or less, the rate limiting steps would be the first ones, i.e., the bimolecular ones. Overall, the sulfoxide reduction process is found to be energetically favorable. Furthermore, our study underscores the significance of dynamic aspects and solvation effects in the catalytic mechanism. These findings enhance our understanding of the molecular basis and thermodynamic activation parameters associated with sulfoxide reduction, but also raise new research questions for further investigations in the msrA enzyme family.

■ CONCLUSIONS

In this study, we exhaustively studied the catalytic mechanism of *Mt*msrA using a combination of experimental and computational methods. Our findings compare, expand, and provide new clues to build a comprehensive picture of this enzyme's behavior. The enzymatic parameters obtained are consistent with previous reports, suggesting that *Mt*msrA has similar enzymatic properties to other members of the msrA family, and the proposed ping-pong type mechanism was confirmed.[54] In several studies, *Ec*trx1 has been utilized as a reductant for msrA,[23,50] but our results revealed that the enzymatic parameters were altered by the choice of the thioredoxin used, highlighting the importance of utilizing physiologically relevant reductants, as previously reported for others msrAs.[59]

The reduction of sulfoxides by thiols has been an area of research for many years, but the catalytic mechanism has not been fully characterized. In particular, various theoretical approaches have been applied for this type of process.[24−26] Our experimental results indicate a strong dependence on the activation process entropy, highlighting the importance of using free energy approaches to accurately estimate the free energy difference and identify the intermediates involved in the process while considering the chemical reaction's dynamics. These simulations usher us to discard the sulfurane species as a possible catalytic intermediate and also to propose an important role for a conserved active site's His residue as an acid−base catalyst (Scheme 2).

Overall, the findings of this study provide new insights into the catalytic and structural characteristics of *Mt*msrA, an important antioxidant enzyme that plays an important role in mycobacteria's survival to oxidative damage. Understanding the mechanism of action of *Mt*msrA and other members of this protein family, will be very helpful to develop new strategies in several research areas, such as organic synthesis, drug discovery, and biotechnology.[60−62]

■ ASSOCIATED CONTENT

Supporting Information

The Supporting Information is available free of charge at https://pubs.acs.org/doi/10.1021/acs.biochem.3c00504.

Initial experimental characterization of *Mt*msrA, msrA catalytic parameter comparison, electronic structure calculations, description of the MD simulated systems, additional pK_a estimations and evolutionary characterization of His155 (PDF)

Accession Codes

The proteins used in this study were *Mt*msrA (UniProt: P9WJM5), *Mt*trxC (Uniprot: P9WG67), *Ec*Trx1 (Uniprot: P0AA25) and *Pa*TR (UniProt: Q9I592).

■ AUTHOR INFORMATION

Corresponding Author

Ari Zeida − *Departamento de Bioquímica, Facultad de Medicina and Centro de Investigaciones Biomédicas (CEINBIO), Facultad de Medicina, Universidad de la República, CP 11800 Montevideo, Uruguay;* orcid.org/0000-0003-0938-287X; Email: azeida@fmed.edu.uy

Authors

Santiago Sastre − *Departamento de Bioquímica, Facultad de Medicina, Departamento de Biofísica, Facultad de Medicina, and Centro de Investigaciones Biomédicas (CEINBIO), Facultad de Medicina, Universidad de la República, CP 11800 Montevideo, Uruguay; Programa de Doctorado en Química, Facultad de Química, Universidad de la República, CP 11800 Montevideo, Uruguay*

Bruno Manta − *Institut Pasteur de Montevideo, CP 11400 Montevideo, Uruguay; Cátedra de Fisiopatología, Facultad de Odontología, Universidad de la República, CP 11600 Montevideo, Uruguay*

Jonathan A. Semelak − *Departamento de Química Inorgánica, Analítica y Química Física, Instituto de Química Física de los Materiales, Medio Ambiente y Energía (INQUIMAE), Facultad de Ciencias Exactas y Naturales, Universidad de Buenos Aires and CONICET, Ciudad Universitaria, CP C1428EGA Buenos Aires, Argentina;* orcid.org/0000-0002-9615-8405

Dario Estrin − *Departamento de Química Inorgánica, Analítica y Química Física, Instituto de Química Física de los Materiales, Medio Ambiente y Energía (INQUIMAE), Facultad de Ciencias Exactas y Naturales, Universidad de Buenos Aires and CONICET, Ciudad Universitaria, CP C1428EGA Buenos Aires, Argentina;* orcid.org/0000-0002-5006-7225

Madia Trujillo − *Departamento de Bioquímica, Facultad de Medicina and Centro de Investigaciones Biomédicas (CEINBIO), Facultad de Medicina, Universidad de la República, CP 11800 Montevideo, Uruguay;* orcid.org/0000-0003-2087-017X

Rafael Radi − *Departamento de Bioquímica, Facultad de Medicina and Centro de Investigaciones Biomédicas (CEINBIO), Facultad de Medicina, Universidad de la República, CP 11800 Montevideo, Uruguay;* orcid.org/0000-0002-1114-1875

Complete contact information is available at: https://pubs.acs.org/10.1021/acs.biochem.3c00504

Notes

The authors declare no competing financial interest.

■ ACKNOWLEDGMENTS

This work was supported by grants of Universidad de la República (CSIC_2018 and EI_2020) to RR. Additional funding was obtained from Programa de Desarrollo de Ciencias Básicas (PEDECIBA, Uruguay) and Programa de Alimentos y Salud Humana (PAyS, IDB-R.O.U. 4950/OC-UR). SS was partially supported by a fellowship from Agencia Nacional de Investigación e Innovación (ANII), Uruguay. JAS

was partially supported by a doctoral fellowship from Consejo Nacional de Investigaciones Científicas y Técnicas (CONICET, Argentina). The simulations presented in this paper were carried out using ClusterUY (site: https://cluster.uy). We thank Dr. Carl F. Nathan (Cornell University, NY, USA) for kindly providing early plasmids for *Mt*msrA expression and purification. We thank Dr. Luis E. S. Netto (Universidade de São Paulo, Brazil) for kindly providing the plasmid for *Pa*TR expression and purification. We thank Dr. Gerardo Ferrer-Sueta from Universidad de la República who kindly provided us with *Ec*Trx1.

■ ABBREVIATIONS

Met, methionine; MetSO, methionine sulfoxide; NAcMet, N-acetyl-L-methionine; NAcMetSO, N-acetyl-L-methionine sulfoxide; H_2O_2, hydrogen peroxide; HOCL, hypochlorous acid; DTT, dithiothreitol; NADPH, reduced nicotinamide adenine dinucleotide phosphate; IPTG, isopro-pyl-β-D-thiogalactopyranoside; Tris, tris(hydroxymethyl)aminomethane; DTPA, diethylenetriaminepentaacetic acid; msr, methionine sulfoxide reductase; dmsA, dimethyl sulfoxide reductase A; bisC, biotin sulfoxide reductase C; trx, thioredoxin; TR, thioredoxin reductase; MBP, maltose-binding protein; *Mt*, *Mycobacterium tuberculosis*; *Pa*, *Pseudomona aeruginosa*; *Ec*, *Escherichia coli*; MD, molecular dynamics; QM/MM, quantum mechanics/molecular mechanics; RESP, restrained electrostatic potential; DFT, density functional theory; PBE, Perdew–Burke–Ernzerhof

■ REFERENCES

(1) Cuq, J. L.; Provansal, M.; Guilleux, F.; Cheftel, C. OXIDATION OF METHIONINE RESIDUES OF CASEIN BY HYDROGEN PEROXIDE. Effects on In Vitro Digestibility. *J. Food Sci.* **1973**, *38*, 11–13.

(2) Pryor, W. A.; Jin, X.; Squadrito, G. L. One- and two-electron oxidations of methionine by peroxynitrite. *Proc. Natl. Acad. Sci. U. S. A.* **1994**, *91*, 11173–11177.

(3) Levine, R. L.; Mosoni, L.; Berlett, B. S.; Stadtman, E. R. Methionine residues as endogenous antioxidants in proteins. *Proc. Natl. Acad. Sci. U. S. A.* **1996**, *93*, 15036–15040.

(4) Armesto, X. L.; Canle L, M.; Fernández, M. I.; Garcıa, M. V.; Santaballa, J. A. First Steps in the Oxidation of Sulfur-Containing Amino Acids by Hypohalogenation: Very Fast Generation of Intermediate Sulfenyl Halides and Halosulfonium Cations. *Tetrahedron* **2000**, *56*, 1103–1109.

(5) John, G. St.; Brot, N.; Ruan, J.; Erdjument-Bromage, H.; Tempst, P.; Weissbach, H.; Nathan, C. Peptide methionine sulfoxide reductase from *Escherichia coli* and *Mycobacterium tuberculosis* protects bacteria against oxidative damage from reactive nitrogen intermediates. *Proc. Natl. Acad. Sci. U. S. A.* **2001**, *98*, 9901–9906.

(6) Peskin, A. V.; Winterbourn, C. C. Kinetics of the reactions of hypochlorous acid and amino acid chloramines with thiols, methionine, and ascorbate. *Free Radic. Biol. Med.* **2001**, *30*, 572–579.

(7) Aledo, J. C. Methionine in proteins: The Cinderella of the proteinogenic amino acids. *Protein Sci.* **2019**, *28*, 1785–1796.

(8) Weissbach, H.; Resnick, L.; Brot, N. Methionine sulfoxide reductases: history and cellular role in protecting against oxidative damage. *Biochim. Biophys. Acta BBA - Proteins Proteomics* **2005**, *1703*, 203–212.

(9) Boschi-Muller, S.; Olry, A.; Antoine, M.; Branlant, G. The enzymology and biochemistry of methionine sulfoxide reductases. *Biochim. Biophys. Acta BBA - Proteins Proteomics* **2005**, *1703*, 231–238.

(10) Binolfi, A.; Limatola, A.; Verzini, S.; Kosten, J.; Theillet, F.-X.; May Rose, H.; Bekei, B.; Stuiver, M.; van Rossum, M.; Selenko, P. Intracellular repair of oxidation-damaged α-synuclein fails to target C-terminal modification sites. *Nat. Commun.* **2016**, *7*, 10251.

(11) Bai, L.; Dong, J.; Liu, Z.; Rao, Y.; Feng, P.; Lan, K. Viperin catalyzes methionine oxidation to promote protein expression and function of helicases. *Sci. Adv.* **2019**, *5*, No. eaax1031.

(12) He, D.; Feng, H.; Sundberg, B.; Yang, J.; Powers, J.; Christian, A. H.; Wilkinson, J. E.; Monnin, C.; Avizonis, D.; Thomas, C. J.; Friedman, R. A.; Kluger, M. D.; Hollingsworth, M. A.; Grandgenett, P. M.; Klute, K. A.; Toste, F. D.; Chang, C. J.; Chio, I. I. C. Methionine oxidation activates pyruvate kinase M2 to promote pancreatic cancer metastasis. *Mol. Cell* **2022**, *82*, 3045–3060.e11.

(13) Park, S.; Trujillo-Hernandez, J. A.; Levine, R. L. Ndufaf2, a protein in mitochondrial complex I, interacts *in vivo* with methionine sulfoxide reductases. *Redox Rep.* **2023**, *28*, 2168635.

(14) Lim, J. M.; Sabbasani, V. R.; Swenson, R. E.; Levine, R. L. Methionine sulfoxide reductases and cholesterol transporter STARD3 constitute an efficient system for detoxification of cholesterol hydroperoxides. *J. Biol. Chem.* **2023**, *299*, 105099.

(15) Ciorba, M. A.; Heinemann, S. H.; Weissbach, H.; Brot, N.; Hoshi, T. Modulation of potassium channel function by methionine oxidation and reduction. *Proc. Natl. Acad. Sci. U. S. A.* **1997**, *94*, 9932–9937.

(16) Manta, B.; Gladyshev, V. N. Regulated methionine oxidation by monooxygenases. *Free Radic. Biol. Med.* **2017**, *109*, 141–155.

(17) Tarafdar, S.; Kim, G.; Levine, R. L. Drosophila methionine sulfoxide reductase A (MSRA) lacks methionine oxidase activity. *Free Radic. Biol. Med.* **2019**, *131*, 154–161.

(18) Peskin, A. V.; Turner, R.; Maghzal, G. J.; Winterbourn, C. C.; Kettle, A. J. Oxidation of Methionine to Dehydromethionine by Reactive Halogen Species Generated by Neutrophils. *Biochemistry* **2009**, *48*, 10175–10182.

(19) Brot, N.; Weissbach, L.; Werth, J.; Weissbach, H. Enzymatic reduction of protein-bound methionine sulfoxide. *Proc. Natl. Acad. Sci. U. S. A.* **1981**, *78*, 2155–2158.

(20) Van Acker, H.; Coenye, T. The Role of Reactive Oxygen Species in Antibiotic-Mediated Killing of Bacteria. *Trends Microbiol.* **2017**, *25*, 456–466.

(21) Piacenza, L.; Trujillo, M.; Radi, R. Reactive species and pathogen antioxidant networks during phagocytosis. *J. Exp. Med.* **2019**, *216*, 501–516.

(22) Shi, L.; Sohaskey, C. D.; North, R. J.; Gennaro, M. L. Transcriptional characterization of the antioxidant response of Mycobacterium tuberculosis in vivo and during adaptation to hypoxia in vitro. *Tuberculosis* **2008**, *88*, 1–6.

(23) Lee, W. L.; Gold, B.; Darby, C.; Brot, N.; Jiang, X.; de Carvalho, L. P. S.; Wellner, D.; St. John, G.; Jacobs, W. R., Jr; Nathan, C. *Mycobacterium tuberculosis* expresses methionine sulfoxide reductases A and B that protect from killing by nitrite and hypochlorite. *Mol. Microbiol.* **2009**, *71*, 583–593.

(24) Balta, B.; Monard, G.; Ruiz-López, M. F.; Antoine, M.; Gand, A.; Boschi-Muller, S.; Branlant, G. Theoretical Study of the Reduction Mechanism of Sulfoxides by Thiols. *J. Phys. Chem. A* **2006**, *110*, 7628–7636.

(25) Thiriot, E.; Monard, G.; Boschi-Muller, S.; Branlant, G.; Ruiz-López, M. F. Reduction mechanism in class A methionine sulfoxide reductases: a theoretical chemistry investigation. *Theor. Chem. Acc.* **2011**, *129*, 93–103.

(26) Dokainish, H. M.; Gauld, J. W. A Molecular Dynamics and Quantum Mechanics/Molecular Mechanics Study of the Catalytic Reductase Mechanism of Methionine Sulfoxide Reductase A: Formation and Reduction of a Sulfenic Acid. *Biochemistry* **2013**, *52*, 1814–1827.

(27) Antoine, M.; Boschi-Muller, S.; Branlant, G. Kinetic Characterization of the Chemical Steps Involved in the Catalytic Mechanism of Methionine Sulfoxide Reductase A from Neisseria meningitidis. *J. Biol. Chem.* **2003**, *278*, 45352–45357.

(28) Coudevylle, N.; Antoine, M.; Boschi-Muller, S.; Branlant, G.; Cung, M.-T. 1H, 13C and 15N Resonance Assignment of an Oxidized

https://doi.org/10.1021/acs.biochem.3c00504
Biochemistry XXXX, XXX, XXX–XXX

form (Cys51-Cys198) of Methionine Sulfoxide Reductase A from Escherichia Coli. *J. Biomol. NMR* **2006**, *36*, 19−19.

(29) Boschi-Muller, S.; Azza, S.; Sanglier-Cianferani, S.; Talfournier, F.; Van Dorsselear, A.; Branlant, G. A Sulfenic Acid Enzyme Intermediate Is Involved in the Catalytic Mechanism of Peptide Methionine Sulfoxide Reductase fromEscherichia coli. *J. Biol. Chem.* **2000**, *275*, 35908−35913.

(30) Lowther, W. T.; Brot, N.; Weissbach, H.; Honek, J. F.; Matthews, B. W. Thiol-disulfide exchange is involved in the catalytic mechanism of peptide methionine sulfoxide reductase. *Proc. Natl. Acad. Sci. U. S. A.* **2000**, *97*, 6463−6468.

(31) Ellman, G. L. Tissue sulfhydryl groups. *Arch. Biochem. Biophys.* **1959**, *82*, 70−77.

(32) Jaeger, T.; Budde, H.; Flohé, L.; Menge, U.; Singh, M.; Trujillo, M.; Radi, R. Multiple thioredoxin-mediated routes to detoxify hydroperoxides in Mycobacterium tuberculosis. *Arch. Biochem. Biophys.* **2004**, *423*, 182−191.

(33) Santos, J.; Marino-Buslje, C.; Kleinman, C.; Ermácora, M. R.; Delfino, J. M. Consolidation of the Thioredoxin Fold by Peptide Recognition: Interaction between *E. coli* Thioredoxin Fragments 1−93 and 94−108. *Biochemistry* **2007**, *46*, 5148−5159.

(34) Taylor, A. B.; Benglis, D. M.; Dhandayuthapani, S.; Hart, P. J. Structure of *Mycobacterium tuberculosis* Methionine Sulfoxide Reductase A in Complex with Protein-Bound Methionine. *J. Bacteriol.* **2003**, *185*, 4119−4126.

(35) Case, D. A.; Walker, R. C.; Cheatham, III, T.; Simmerling, C.; Roitberg, A.; Merz, K. M.; Luo, R.; Darden, T.; Wang, J.; Duke, R. E.; Roe, D. R.; LeGrand, S.; Swails, J.; Götz, A. W.; Smith, J.; Cerutti, D.; Brozell, S.; Luchko, T.; Cruzeiro, V. W. D.; Ghoreishi, D.; Monard, G.; Sagui, C.; Pan, F.; Cisneros, G. A.; Miao, Y.; Shen, J.; Harris, R.; Huang, Y.; Lin, C.; Mermelstein, D.; Li, P.; Onufriev, A.; Izadi, S.; Wolf, R. M.; Wu, X.; Gohlke, H.; Schott-Verdugo, S.; Homeyer, N.; Qi, R.; Xiao, L.; Wei, H.; Greene, D.; Lee, T.; York, D.; Liu, J.; Nguyen, H.; Omelyan, I.; Kovalenko, A.; Gilson, M.; Ben-Shalom, I.; Nguyen, C.; Salomon-Ferrer, R.; Kurtzman, T.; Kollman, P. A. AMBER 2018. University of California, San Francisco, 2018.

(36) Maier, J. A.; Martinez, C.; Kasavajhala, K.; Wickstrom, L.; Hauser, K. E.; Simmerling, C. ff14SB: Improving the Accuracy of Protein Side Chain and Backbone Parameters from ff99SB. *J. Chem. Theory Comput.* **2015**, *11*, 3696−3713.

(37) Bayly, C. I.; Cieplak, P.; Cornell, W.; Kollman, P. A. A well-behaved electrostatic potential based method using charge restraints for deriving atomic charges: the RESP model. *J. Phys. Chem.* **1993**, *97*, 10269−10280.

(38) Cornell, W. D.; Cieplak, P.; Bayly, C. I.; Kollman, P. A. Application of RESP charges to calculate conformational energies, hydrogen bond energies, and free energies of solvation. *J. Am. Chem. Soc.* **1993**, *115*, 9620−9631.

(39) Wang, J.; Wolf, R. M.; Caldwell, J. W.; Kollman, P. A.; Case, D. A. Development and testing of a general amber force field. *J. Comput. Chem.* **2004**, *25*, 1157−1174.

(40) Essmann, U.; Perera, L.; Berkowitz, M. L.; Darden, T.; Lee, H.; Pedersen, L. G. A smooth particle mesh Ewald method. *J. Chem. Phys.* **1995**, *103*, 8577−8593.

(41) Ryckaert, J.-P.; Ciccotti, G.; Berendsen, H. C. P. Numerical integration of the Cartesian Equations of Motion of a System with Constraints: Molecular Dynamics of n-Alkanes. *J. Comput. Phys.* **1977**, *23*, 327−341.

(42) Socher, E.; Sticht, H. Mimicking titration experiments with MD simulations: A protocol for the investigation of pH-dependent effects on proteins. *Sci. Rep.* **2016**, *6*, 22523.

(43) Nitsche, M. A.; Ferreria, M.; Mocskos, E. E.; González Lebrero, M. C. GPU Accelerated Implementation of Density Functional Theory for Hybrid QM/MM Simulations. *J. Chem. Theory Comput.* **2014**, *10*, 959−967.

(44) Marcolongo, J. P.; Zeida, A.; Semelak, J. A.; Foglia, N. O.; Morzan, U. N.; Estrin, D. A.; González Lebrero, M. C.; Scherlis, D. A. Chemical Reactivity and Spectroscopy Explored From QM/MM Molecular Dynamics Simulations Using the LIO Code. *Front. Chem.* **2018**, *6*, 70.

(45) Perdew, J. P.; Burke, K.; Ernzerhof, M. Generalized Gradient Approximation Made Simple. *Phys. Rev. Lett.* **1996**, *77*, 3865−3868.

(46) Kästner, J. Umbrella sampling: Umbrella sampling. *Wiley Interdiscip. Rev. Comput. Mol. Sci.* **2011**, *1*, 932−942.

(47) Zeida, A.; Reyes, A. M.; Lebrero, M. C. G.; Radi, R.; Trujillo, M.; Estrin, D. A. The extraordinary catalytic ability of peroxiredoxins: a combined experimental and QM/MM study on the fast thiol oxidation step. *Chem. Commun.* **2014**, *50*, 10070−10073.

(48) Zeida, A.; Reyes, A. M.; Lichtig, P.; Hugo, M.; Vazquez, D. S.; Santos, J.; González Flecha, F. L.; Radi, R.; Estrin, D. A.; Trujillo, M. Molecular Basis of Hydroperoxide Specificity in Peroxiredoxins: The Case of AhpE from *Mycobacterium tuberculosis*. *Biochemistry* **2015**, *54*, 7237−7247.

(49) Humphrey, W.; Dalke, A.; Schulten, K. VMD: Visual molecular dynamics. *J. Mol. Graph.* **1996**, *14*, 33−38.

(50) Antoine, M.; Gand, A.; Boschi-Muller, S.; Branlant, G. Characterization of the Amino Acids from Neisseria meningitidis MsrA Involved in the Chemical Catalysis of the Methionine Sulfoxide Reduction Step. *J. Biol. Chem.* **2006**, *281*, 39062−39070.

(51) Ranaivoson, F. M.; Antoine, M.; Kauffmann, B.; Boschi-Muller, S.; Aubry, A.; Branlant, G.; Favier, F. A Structural Analysis of the Catalytic Mechanism of Methionine Sulfoxide Reductase A from Neisseria meningitidis. *J. Mol. Biol.* **2008**, *377*, 268−280.

(52) Olry, A.; Boschi-Muller, S.; Marraud, M.; Sanglier-Cianferani, S.; Van Dorsselear, A.; Branlant, G. Characterization of the Methionine Sulfoxide Reductase Activities of PILB, a Probable Virulence Factor from Neisseria meningitidis. *J. Biol. Chem.* **2002**, *277*, 12016−12022.

(53) Lim, J. C.; Gruschus, J. M.; Kim, G.; Berlett, B. S.; Tjandra, N.; Levine, R. L. A Low pK Cysteine at the Active Site of Mouse Methionine Sulfoxide Reductase A. *J. Biol. Chem.* **2012**, *287*, 25596−25601.

(54) Boschi-Muller, S.; Azza, S.; Branlant, G. E. coli methionine sulfoxide reductase with a truncated N terminus or C terminus, or both, retains the ability to reduce methionine sulfoxide. *Protein Sci.* **2001**, *10*, 2272−2279.

(55) Jencks, W. P. Requirements for general acid-base catalysis of complex reactions. *J. Am. Chem. Soc.* **1972**, *94*, 4731−4732.

(56) Luo, D.; Smith, S. W.; Anderson, B. D. Kinetics and Mechanism of the Reaction of Cysteine and Hydrogen Peroxide in Aqueous Solution. *J. Pharm. Sci.* **2005**, *94*, 304−316.

(57) Ashby, M. T.; Nagy, P. On the kinetics and mechanism of the reaction of cysteine and hydrogen peroxide in aqueous solution. *J. Pharm. Sci.* **2006**, *95*, 15−18.

(58) Zhao, Y.; Truhlar, D. G. Density Functionals with Broad Applicability in Chemistry. *Acc. Chem. Res.* **2008**, *41*, 157−167.

(59) Napolitano, S.; Reber, R. J.; Rubini, M.; Glockshuber, R. Functional analyses of ancestral thioredoxins provide insights into their evolutionary history. *J. Biol. Chem.* **2019**, *294*, 14105−14118.

(60) Nosek, V.; Míšek, J. Enzymatic kinetic resolution of chiral sulfoxides - an enantiocomplementary approach. *Chem. Commun.* **2019**, *55*, 10480−10483.

(61) Wen, Y.; Peng, L.; Zhou, Y.; Peng, T.; Chen, Y.; Cheng, X.; Chen, Y.; Yang, J. Discovery and application of methionine sulfoxide reductase B for preparation of (S)-sulfoxides through kinetic resolution. *Catal. Commun.* **2020**, *136*, 105908.

(62) Zhao, Y.; Jiang, X.; Zhou, S.; Tian, J.; Yang, P.; Chen, Y.; Zhang, Q.; Xu, X.; Chen, Y.; Yang, J. Kinetic resolution of sulfoxides with high enantioselectivity using a new homologue of methionine sulfoxide reductase B. *Org. Biomol. Chem.* **2023**, *21*, 3417−3422.

https://doi.org/10.1021/acs.biochem.3c00504
Biochemistry XXXX, XXX, XXX−XXX